Expanded Pass stopping code

Schinner, Andreas; Sigmund, Peter

Published in:
Nuclear Instruments and Methods in Physics Research Section B: Beam Interactions with Materials and Atoms

DOI:
10.1016/j.nimb.2018.10.047

Publication date:
2019

Document version:
Submitted manuscript

Citation for pulished version (APA):
Schinner, A., & Sigmund, P. (2019). Expanded Pass stopping code. *Nuclear Instruments and Methods in Physics Research Section B: Beam Interactions with Materials and Atoms*, *460*, 19-26.
https://doi.org/10.1016/j.nimb.2018.10.047

Expanded PASS Stopping Code

A. Schinner[a], P. Sigmund[b]

[a]*Department of Experimental Physics, Johannes Kepler University, A-4040 Linz, Austria*
[b]*Department of Physics, Chemistry and Pharmacy, University of Southern Denmark, DK-5230 Odense M, Denmark*

Abstract

The first version of the PASS code was developed in 2000 on the basis of binary theory of electronic stopping, a generalization of Niels Bohr's 1913 theory of the stopping of alpha particles in matter. The code has been applied in a number of fundamental studies of energy-loss problems, including Barkas-Andersen effect and straggling as well as channeling and electron emission, and it underlies the ICRU tabulation of stopping data for ions with atomic numbers 3-16 in 25 elementary and 32 compound materials over an energy range from 25 keV/u to 1 GeV/u.

We report about a major expansion of the code, so that mean energy losses can be computed for 92 ions in 92 elemental targets. Comparisons with measurements have been made over the entire energy range for which experimental data are listed in the IAEA database.

The code allows to compute energy losses for arbitrary compound target materials by assuming Bragg additivity. Predictions beyond the Bragg rule are available for selected materials.

In this paper we specify the underlying physics and improvements of the code during the period since its first implementation. Strengths and weaknesses are demonstrated graphically for a number of ion-target combinations. Tables for 92×92 ion-target combinations over an energy range from 1 keV/u to 1 GeV/u are freely accessible on the internet in the DPASS (Dataset PASS) code.

Keywords: Stopping power, Binary theory, PASS code, DPASS code

Email address: sigmund@sdu.dk (P. Sigmund)

1. Introduction

Quantitative data characterizing the energy loss of energetic charged particles in matter are essential in all applications of accelerators. The central parameter is the mean energy loss per pathlength, commonly characterized by the stopping force (or stopping power) dE/dR or the stopping cross section

$$S = -\frac{1}{N}\frac{dE}{dR}, \tag{1}$$

where N is the number of atoms or molecules per target volume.

A large number of data has been accumulated since the first experimental studies early in the past century. New experimental data are being reported year for year and are being compiled in a database listing the results of more than a thousand studies [1]. Numerous parametrizations of these results, guided in part by theory, have been condensed in tabular form, of which we mention [2, 3, 4, 5, 6, 7, 8].

At the same time, stopping of charged particles has been and still is an active research area within theoretical atomic and condensed-matter physics. Among numerous reviews we mention [9, 10, 11, 12]. Theoretical considerations have contributed significantly to the ICRU tables for protons and alpha particles [7]. ICRU tables for ions heavier than helium [13] are theory-based but need input in the form of empirical data for atomic properties. The same holds for the CasP code [14] which provides stopping data for a very wide range of ions, targets and energies.

With the present paper we follow the request by numerous users of accelerators to make PASS output easily accessible. One reason for the long delay to follow this request was the limited number of target elements for which reliable input data, primarily oscillator-strength spectra over a wide frequency range, are available. Another critical point is noticeable discrepancies between PASS predictions and experimental data in the velocity range around and below the Bohr speed v_0, i.e., in an energy range of central importance in numerous applications of ion beams such as micro, nano and fusion technology.

We have now found ways to overcome these obstacles and, consequently, have established a standard version of PASS which we hope will become useful for applications in science and technology. Output of this code has been compiled in a program DPASS, which allows instant delivery of stopping data for a given ion-target combination amongst all 92×92 pairs of elements for a specified range of beam energies within the interval between 1 keV/u and 1 GeV/u [15].

After a brief recapitulation of binary stopping theory [16] and later developments in Sect. 2 we specify in some detail the procedure leading to the stopping tables in Sect. 3. Output is illustrated in a number of representative graphs in Sect. 4.

2. Recapitulation of Binary Stopping Theory

2.1. Basics

Binary stopping theory [16] is an extension of Niels Bohr's classical theory of 1913 [17]. Bohr considered the interaction of a swift point charge with independent electrons bound harmonically to a target nucleus. A distinction was made between close (small impact parameter) collisions which were described by free-Coulomb scattering, and distant collisions characterized by forced oscillators initiated by the Coulomb force from a uniformly moving point charge. In essence, the binding force causes the Coulomb force between the ion and the target electron to be screened to within the so-called adiabatic radius $a_{\rm ad} = v/\omega$, where ω is the resonance frequency of the oscillator modeling an individual electron.

Lindhard [18] went a step further and replaced the binding force by changing the Coulomb interaction potential between the ion and a target electron into a Yukawa potential with the adiabatic radius serving as a screening radius. This had the effect that the stopping cross section became dependent on the sign of the projectile charge, an effect that had been found experimentally long ago by Barkas and coworkers [19] and was demonstrated to affect the stopping of swift ions by Andersen et al. [20]. In essence, the stopping cross section of an ion with atomic number Z_1 was taken to be proportional to Z_1^2 in accordance with Bethe's quantum theory [21] and amended by a Barkas-Andersen correction $\propto Z_1^3$.

In binary stopping theory [16], Lindhard's idea is taken beyond an expansion in powers of Z_1. Here the interaction between the projectile and a target electron is described by the full classical scattering integral for a Yukawa potential. In this way there is a smooth transition between close and distant interactions, and a Barkas-Andersen correction is inherent in the theory.

The classical scattering integral describes kinetic-energy transfer to a target electron, but Bohr theory also includes transfer of potential energy to the oscillator. In binary theory this contribution is described in terms of angular-momentum transfer. Somewhat surprisingly, this equivalence was found to be exact for Yukawa-type interaction [16] at least for distant collisions.

The model so defined constitutes the kernel of the PASS stopping code. It delivers the energy transfer to one target electron that is initially at rest as a function

of the impact parameter and, after integration, the stopping cross section versus beam velocity or energy.

According to Bohr [9] the range of validity of this picture is limited by the condition that

$$\kappa = \frac{2Z_1 e^2}{\hbar v} > 1. \tag{2}$$

Conversely, the range of validity of Bethe's quantum theory [21] is defined by the Sommerfeld criterion $Z_1 e^2/\hbar v < 1$. The transition between these two regimes is conventionally described in terms of the Bloch correction [22] to the Bethe theory. In binary theory this transition is described by an inverse-Bloch correction to the extended Bohr theory [23].

2.2. PASS Code

2.2.1. Modeling the Atom

In Bohr stopping theory the atom is characterized by Z_2 electrons with a set of resonance frequencies ω_j. In Bethe theory [21] this picture is generalized to a spectrum of oscillator strengths. In accordance with common practice, PASS characterizes target atoms by a discrete spectrum of oscillator strengths f_j satisfying the sum rule

$$\sum_j f_j = Z_2, \tag{3}$$

where j denotes individual shells and/or subshells, for which there is specified a resonance frequency $\omega_j = I_j/\hbar$ defined by

$$\ln I_j = \frac{\int_j d(\hbar\omega) f(\hbar\omega) \ln(\hbar\omega)}{\int_j d(\hbar\omega) f(\hbar\omega)}, \tag{4}$$

where $\int_j$ denotes the integral over that portion of the continuous oscillator-strength spectrum which is associated with the jth shell/subshell. In other words, I_j is the equivalent of the mean logarithmic excitation energy or "I-value" in the Bethe theory for shell j. In addition to I_j-values we also need shell binding energies (ionization potentials) U_j. These quantities limit the potential-energy transfer, since energy transferred beyond the ionization energy must be kinetic.

PASS offers two ways to determine I_j-values:

- For all elements covered in [13], oscillator-strength spectra extracted from [24, 25, 26, 27] were discretized, guided by absorption edges, nominal occupation numbers of principal and/or subshells and the sum rule (3),

- Alternatively, I_j-values can be determined by the SBS scheme [28], where f_j is taken to be the nominal occupation number of the shell or subshell and I_j is taken to be $= \alpha U_j$, with α defined so that

$$\sum_j f_j \ln I_j = Z_2 \ln I, \tag{5}$$

where I is the total I-value which, for this option, is the only input quantity besides the shell binding energies U_j. The factor α was introduced originally as a fitting parameter [29] between adopted values of I_j and U_j. In ref. [28], a simple theoretical estimate led to the value $\alpha = \sqrt{e} = 1.649$ for all elements. Our assumption of α being a constant for all subshells of a given element is intermediate between these two approaches.

2.2.2. The Projectile

In accordance with Bohr and Bethe theory, binary stopping theory treats the motion of the projectile as uniform. In addition to the dynamic screening characterized by the adiabatic radius, additional screening is due to electrons bound to the penetrating ion. Moreover, excitation of these electrons gives rise to additional loss of kinetic energy by the projectile, and so does charge exchange.

The screened ion-electron interaction potential is taken as

$$V(r) = -\frac{q_1 e^2}{r}\, e^{-r/a_{\rm ad}} - \frac{(Z_1 - q_1)e^2}{r}\, \chi(r/a), \tag{6}$$

where r denotes the distance between the projectile nucleus and the target electron, q_1 is the ion charge, $\chi(r/a)$ a screening function, $a_{\rm ad} = v/\omega$ the adiabatic radius and

$$\frac{1}{a^2} = \frac{1}{a_{\rm ad}^2} + \frac{1}{a_{\rm sc}^2}. \tag{7}$$

The screening radius $a_{\rm sc}$ is given by [30]

$$a_{\rm sc} = a_{\rm TF} \left(1 - \frac{q_1}{Z_1}\right)^{\mathsf{r}}, \tag{8}$$

where $a_{\rm TF} = 0.8853 a_0 / Z_1^{1/3}$ and r is a numerical coefficient with the default value 1.

For the screening function the default is

$$\chi(r/a) = e^{-r/a}, \tag{9}$$

but also Molière screening [31] is an option.

PASS offers two basic options for the projectile charge, either a frozen charge which can be anywhere between 0 and $Z_1 e$, or an equilibrium charge dependent primarily on the beam velocity. Several options are offered for the latter,

1. a simple Thomas-Fermi-type charge function,

$$q_1 = Z_1 e \left(1 - e^{-v/v_{\mathrm{TF}}}\right), \tag{10}$$

   where $v_{\mathsf{TF}} = v_0 Z_1^{2/3}$ and v_0 is the Bohr speed,
2. a fitting formula approximating the genuine Thomas-Fermi charge state [12],

$$q_1 = Z_1 \frac{1 - e^{-1.43 v/v_{\mathsf{TF}}}}{1 + e^{-3.56 v/v_{\mathsf{TF}}}}, \tag{11}$$

3. an evaluation of the Lamb criterion [32] based on tabulated binding energies [33],
4. a modified Thomas-Fermi formula,

$$q_1 = Z_1 \left(1 - e^{-Av/Z_1^{0.45} v_0}\right)^C \tag{12}$$

   with parameters A, C that can be chosen to match a given charge-state function,
5. The Shima formula [34]

$$q_1 = Z_1 \left(1 - e^{-1.25X + 0.32X^2 - 0.11X^3}\right) F(Z_2, X) \tag{13}$$

$$F(Z_2, X) = 1 - 0.0019(Z_2 - 6)\sqrt{X} + 0.00001(Z_2 - 6)^2 X \tag{14}$$

   with or without the correction factor $F(Z_2, X)$, where $X = 0.608 v/Z_1^{0.45} v_0$, and
6. formulae by Schiwietz & Grande [35] for gas and solid targets.

On the basis of extensive comparisons of these options with measured stopping cross sections we have found that the simplest option, Eq. (10), which we adopted in generating the tables in ref. [13], represents the best overall solution over a wide range of energies and atomic numbers. In specific cases, where a reliable expression for the mean charge state or experimental data exists, option 12 may be appropriate. We have applied this option in ref. [36].

2.2.3. Projectile Excitation

Projectile excitation is treated in analogy with target excitation by viewing the collision event from a reference frame moving with the projectile, taking due account of the charge state. An important difference is that the energy lost in projectile ionization is taken to be the ionization energy U_j of the pertinent shell, while additional energy received by a liberated electron may just as well accelerate as slow down the projectile, depending on the direction of its momentum [37].

PASS offers two options for the electron configuration in a partially stripped ion,

- Energy levels are occupied from the bottom up, or
- All energy levels of the neutral atom are occupied, but all oscillator strengths are reduced by a factor $(Z - q)/Z$.

The second solution, called 'distributed', accounts approximately for the fact that an ion in motion is typically not in its ground state. While this model is admittedly crude, the difference between the two options is small in practice. Moreover, projectile excitation itself is a relatively small effect.

2.2.4. Energy Loss by Electron Capture and Loss

Cross sections for electron loss can readily determined by PASS, but cross sections for charge exchange have not been included so far. However, in charge equilibrium, the energy lost in a capture-loss cycle is determined by the cross section for projectile ionization and the requirement that cross sections for capture and loss must be equal. This option is included in PASS.

2.2.5. Shell Correction

Shell corrections account for the orbital motion of target electrons in their initial state. This effect is not present in the original Bohr theory but has been considered much later [38]. The effect is taken fully into account in the formalism leading to Bethe's quantum theory [21] but ignored in the final formula. Shell corrections were subsequently allowed for by adding terms to the stopping number of inner-shell electrons [39]. Fano formulated shell corrections as an additive term in the form of an expansion in powers of $\langle v_e^2 \rangle / v^2$ [10], where v_e denotes the orbital speed of a target electron.

PASS introduces shell corrections by a procedure proposed in [40], which represents a convolution of the stopping cross section for a stationary target electron with the velocity distributions of the individual orbital. PASS offers two options

based on either hydrogenic or Hartree-Fock orbitals, the latter based on [41] for $Z_1 \leq 54$ and [42] for $Z_1 > 54$.

2.2.6. Relativity

Relativistic effects enter at several stages. Relativistic kinematics has been treated both in Bohr's [43] and Bethe's stopping theories [44], with slightly different results. For light ions the relativistic range falls into the Bethe regime. Therefore we have incorporated the Bethe expression as the standard relativistic correction.

For heavy ions Lindhard & Sørensen [45] established an extension of the Bethe theory incorporating several pertinent effects, including a relativistic Bloch correction and deviations from Coulomb interaction in view of the finite size of the nucleus. This Lindhard-Sørensen correction has been incorporated into PASS.

2.2.7. Compound Targets

PASS allows two options for computing stopping cross sections of compound materials,

- the so-called Bragg additivity rule [46],

$$S(X_a, Y_b \dots) = C_a S_X + C_b S_Y \dots, \tag{15}$$

  where C_a is the fraction of X-atoms, i.e., $a/(a + b + \dots)$ or

- assigning a modified spectrum of oscillator strengths to a compound. In practice this is done by keeping the resonance frequencies of the elements involved but changing the occupation numbers in accordance with the chemical structure. As an example, for NaCl occupation numbers for inner shells are kept unchanged in both atoms, but the single valence electron in Na will be added to the Cl atom, so that both atoms appear as a Ne-Ar pair, except for the I-value of the transferred electron. This option was employed for some compunds in [13] and more recently in ref. [47].

2.3. Applications

Pass has been coded to produce several kinds of output,

- Stopping numbers, stopping cross sections or stopping forces as a function of beam velocity [23, 13],

- Energy-loss spectra and secondary-electron emission spectra in ion-atom collisions [48, 49],
- Linear energy-loss straggling, i.e., collisional straggling due to isolated target electrons [50],
- Impact-parameter-dependent energy loss [51] with application to channeling [52] as well as correlated straggling, i.e., bunching and packing caused by the proximity of target electrons [53],
- Analysis of stopping measurements in transmission [54].

3. The DPASS Code

DPASS is a compilation of stopping cross sections based on PASS that is freely accessible on the internet [15]. In this section we specify the package of options that have been applied in compiling the underlying tables.

3.1. Oscillator Spectrum

Oscillator spectra (f_j, ω_j) have been prepared for all subshells of elements $Z = 1 \ldots 92$ by means of the SBS scheme specified in Section 2.2.1.

I-values have been determined on the basis of stopping cross sections for MeV protons in selected target materials. In principle this is the procedure underlying all existing comprehensive tabulations such as [55] and [7]. The procedure applied here is based on the PASS code which incorporates shell and Barkas-Andersen corrections from the beginning.

In practice we relied on stopping cross sections reported from Risø ([56] and later references from the same group compiled in [1]) and Nara ([57] and later references from the same group compiled in [1]). A program ISBS was written that runs PASS for a series of I-values and minimizes the rms deviation from a given set of data over a predefined energy interval. The lower energy limit was set to 1 MeV. As is seen in the upper graph of Figure 1, there is generally good agreement between Risø and Nara data, while there are noticeable deviations from the ICRU49 data mainly for Z-values above 40.

The lower graph in Figure 1 shows the set of I-values underlying the current version of DPASS compared with the values from [7]. We used data from Risø or Nara where available, and where data from both sources are available we took the average. Missing I-values were filled in by linear interpolation. Gas data were treated separately, because both Risø and Nara measurements concern solid

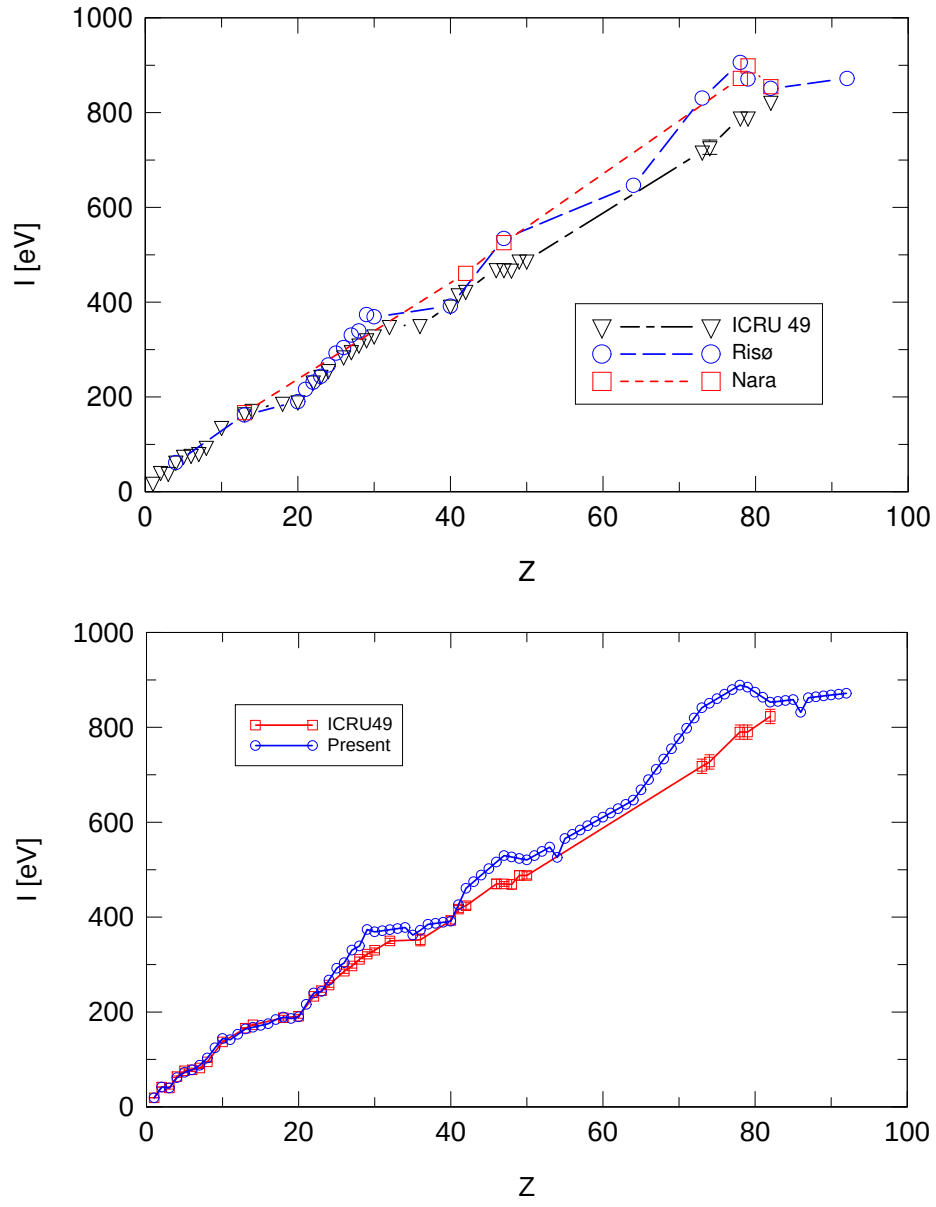

Figure 1: I-values determined by analysis of proton stopping data. Top: Data from Risø and Nara compared with values recommended by ICRU [7]. Bottom: Data adopted for the current version of DPASS compared with ICRU49 data.

targets. For H and He, standard I-values have been taken. For Z from 5 up to 36 we applied ISBS to stopping cross sections compiled in [1], and for $Z = 54$ and 86 we adopted ICRU values from [7].

3.2. Shell correction

Shell corrections have been evaluated element by element on the basis of ref. [40] via velocity distributions determined from [41] up to $Z = 54$ and from [42] for higher Z. The fact that relativity is ignored in these tabulations is a source of error for heavy target and projectile atoms, which we intend to eliminate in a later version of DPASS. We note, however, that relativity is fully accounted for in the basic PASS code, and that ignoring relativity in the determination of I-values mainly affects the innermost shells which, for high-Z targets, only contribute a minor portion of the stopping cross section.

3.3. Conductors

For metals, PASS treats the valence shell as a free electron gas. Standard schemes like ref. [58] are limited to light projectiles such as protons and electrons. Instead, a classical description of the electron gas has been used from the very beginning [23] with the plasma frequency reflecting the density of conduction electrons defining the I-value of the outermost shell. The shell correction for conduction electrons is determined via the Fermi-Dirac distribution.

PASS also allows to treat the valence shell of bound atoms with the aim of comparing the stopping in metal vapor with stopping in a metal. However, DPASS only considers metal targets in the solid state.

3.4. Remaining Options

For most of the remaining options we used the defaults in the current version of DPASS. Specifically we mention the following:

- Equilibrium ion charge: The simple Thomas-Fermi expression (10),
- Projectile screening: Exponential,
- Projectile configuration: Distributed.

3.5. User Interface

DPASS is a Windows program freely available from [15] and easy to install. It delivers stopping cross sections for $Z_{1,2} = 1 \ldots 92$ in units of 10^{-15}eVcm^2, MeVcm^2/mg or eV/nm over a chosen grid of energies between 0.001 and 1000 MeV/u.

4. Examples

4.1. Solid Targets

Figure 2 shows stopping cross sections for several ions in Al, Ag and Au (top to bottom) over the energy range for which data are found in the IAEA database [1]. Near and above the stopping maximum we find full agreement with the PASS curves within experimental scatter. This has to be so for H ions, since those data have served to determine the I-values of these three metals. The fact that similarly good agreement is found for ions up to U supports the theoretical scheme, in particular the screening model and the Barkas-Andersen correction. We note that at 10 MeV/u the equilibrium charge of a uranium ion is 58 according to Eq. (10), i.e., we are still far away from a point projectile.

At lower beam energies the situation changes markedly. In a few cases such as O-Al as well as part of the data for H and He in Ag and Au we see near-perfect agreement with the PASS curves, but the bulk of the data lies *below* the PASS predictions. We come back to this point below.

Figure 3 shows similar data for C and Si targets. Again we find excellent agreement between theory and existing data at energies above the stopping maximum. There are minor deviations, 10-20%, in the stopping maximum. Again, some of the data, like C and O in C as well as C and Xe in Si, fall right on the theoretical curves, and for both H and He in Si there are data close to theory and others far away.

4.2. Nitrogen target

We have studied stopping in gas targets, especially He, Ne and Ar extensively in two recent papers [59, 60]. Therefore we here only consider nitrogen as a target. For energies around and above the stopping maximum the same observations can be made as for C and Si. For H ions we find relatively good agreement also at low energies with the data, better than 20%, if five low-lying data points at the low-energy end, taken on solid nitrogen targets [61] are considered separately. Dramatic differences, up to a factor of three, are found for He, Li and, in particular, Ne ions at the low-energy end.

4.3. Heavy Ions

Figures 5 and 6 show comparisons between stopping cross sections for Xe, Au, Pb and U ions and data from the IAEA compilation [1]. There are not many data for these heavy ions, and most of those are included in the plots. While for xenon ions we still find perfect agreement between theory and measurements above the

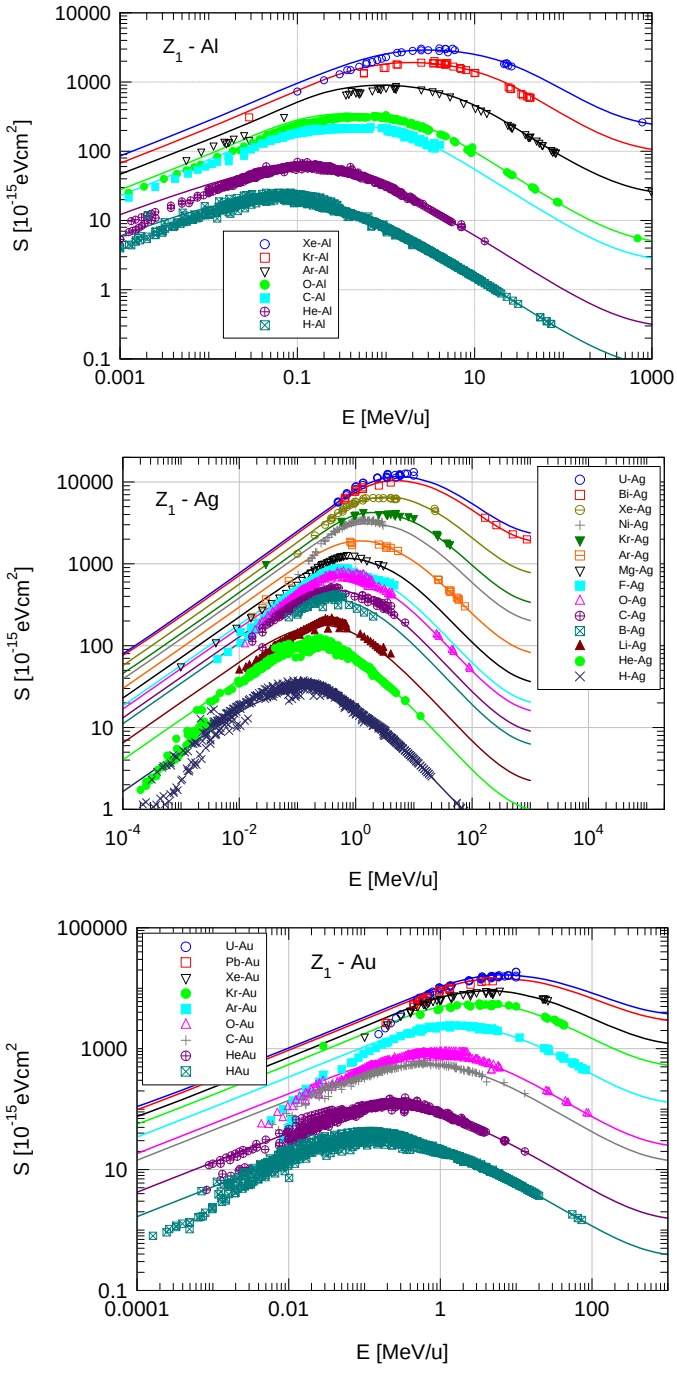

Figure 2: Stopping cross sections from PASS for Al, Ag and Au targets (top to bottom) compared with data from the Paul compilation [1]

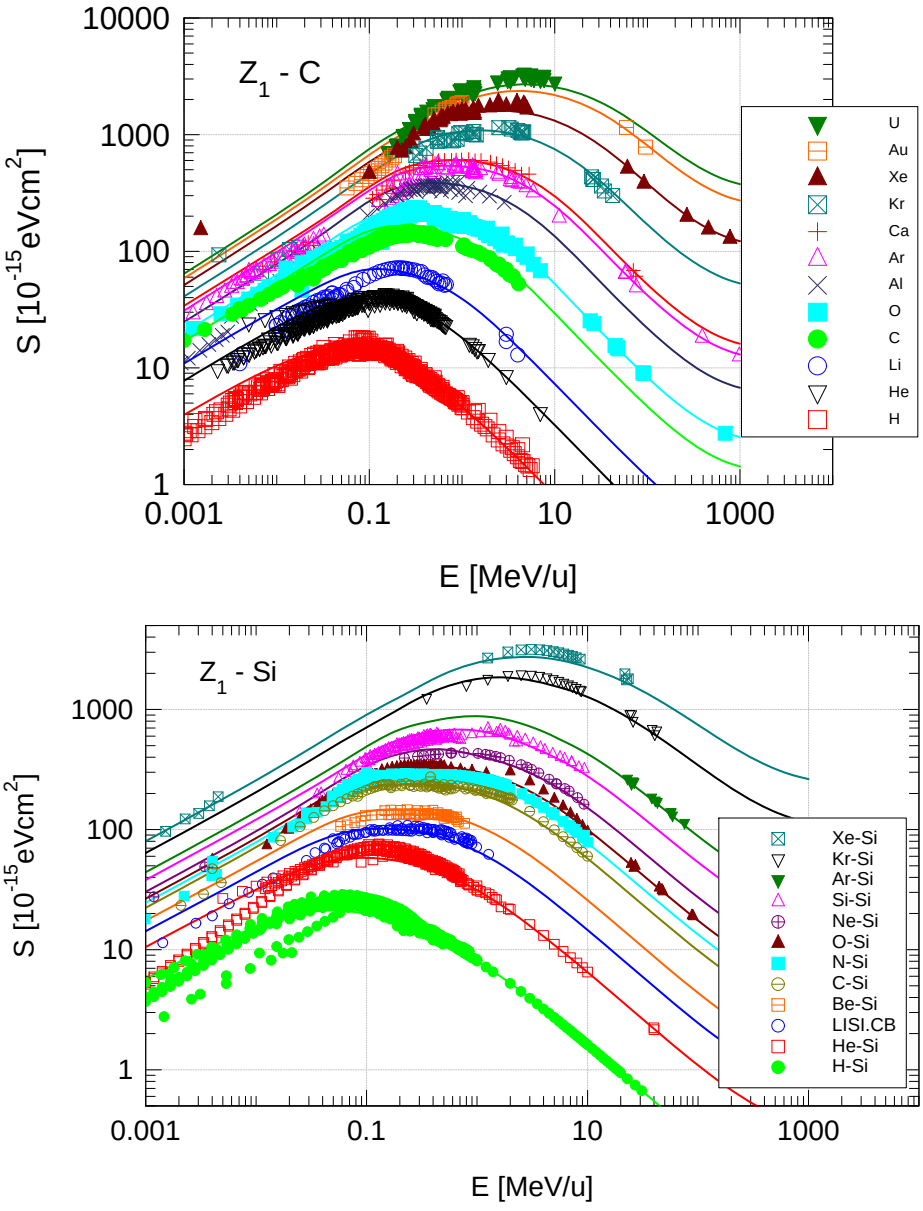

Figure 3: Same as figure 2 for C (top) and Si (bottom).

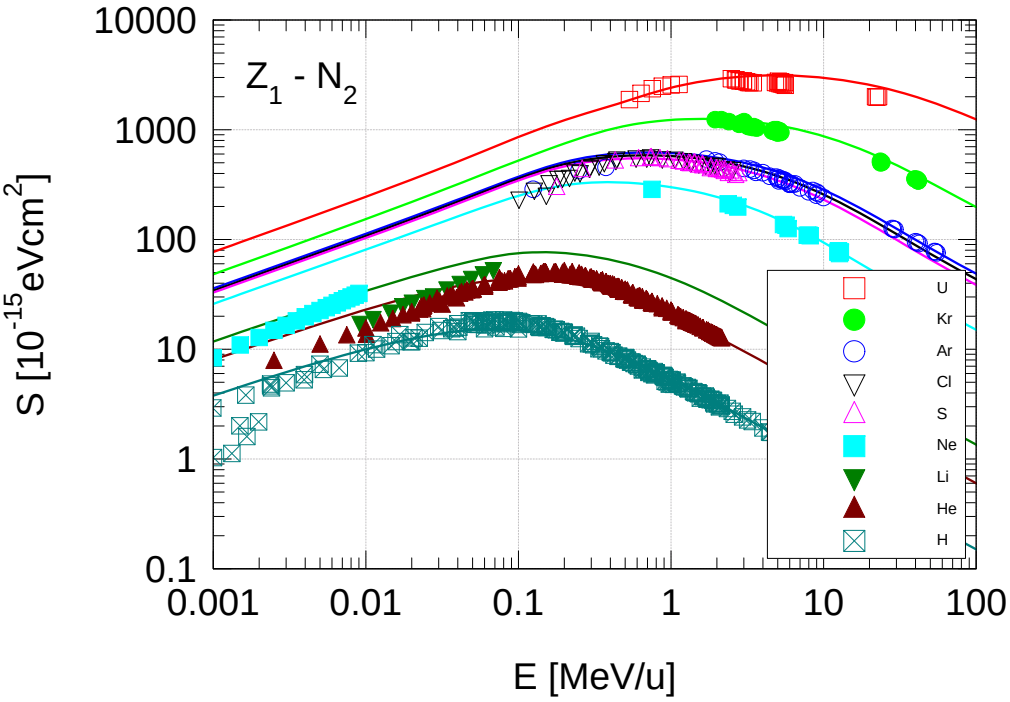

Figure 4: Same as Figure 2 for nitrogen target.

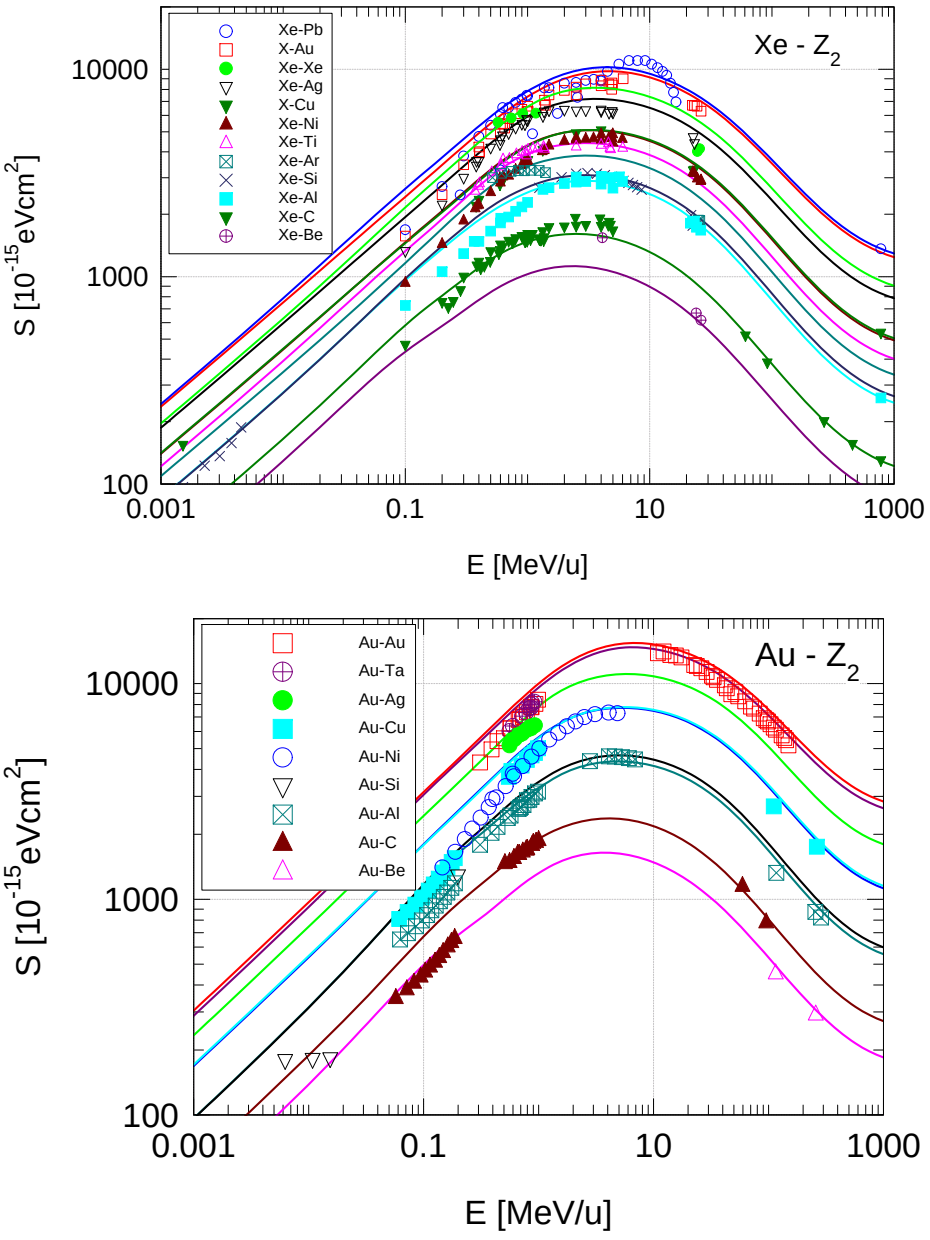

Figure 5: Stopping cross sections from PASS for Xe and ions compared with data from the Paul compilation [1]

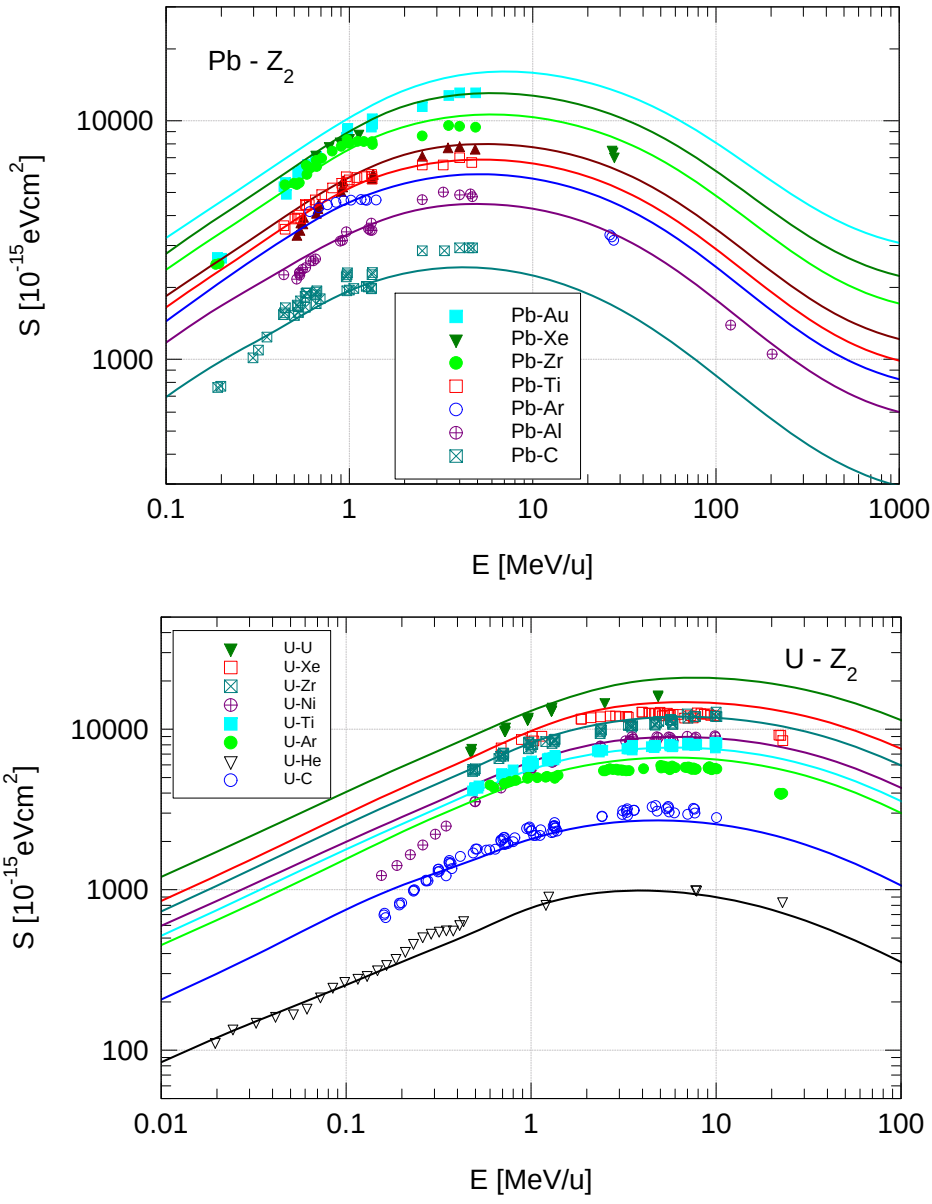

Figure 6: Same as Figure 5 for Pb and U ions

stopping maximum, discrepancies of up to 20-30% are found in the peak region. Differences at low energies are similar to those found in the previous graphs, but we note that also here, experimental data lie *below* the predictions.

For gold ions (Figure 5, lower graph) we still find acceptable agreement at energies down to slightly below 1 MeV/u, but further down all plotted data deviate by 30% or more from the predictions. For lead ions (Figure 6, upper graph) significant deviations, $\sim 20\%$, are already found in the energy range around the maximum, and similarly for U ions in the lower graph.

5. Discussion

Considering the breadth of coverage in terms of beam energy and atomic numbers we find the degree of agreement between DPASS output and experimental data promising. However, there are discrepancies, some of which appear systematic. Therefore we find it useful to summarize possible reasons for those with a view to further development of the code. We divide this discussion into aspects of the PASS code and experimental aspects.

5.1. The PASS Code

5.1.1. Oscillator strength spectrum and I-values

The weakest point in our adopted oscillator-strength spectrum is the interpolation of I-values for $Z > 30$ shown in Figure 1. This does not seem to have dramatic consequences on the graphs shown here, since those materials where reliable I-values have been determined are, by and large, those for which there exist reliable stopping data. However, establishing a narrower grid of reliable I-values is an obvious item on our road map.

Errors originating from the adoption of the SBS scheme to determine oscillator-strength spectra (f_j, ω_j) are negligible in the Bethe regime, where the total I-value is the dominating input. There is an influence at lower energies, but the dramatic discrepancies seen in some of our graphs have a different origin, as discussed below. We note that also the alternative procedure that led to the spectra utilized in ref. [13] is not free of ambiguities, especially with regard to the treatment of outer shells which govern stopping at low energies.

5.1.2. Shell correction

While the theoretical basis of our shell corrections [40] is widely accepted, the use of nonrelativistic wave functions [42] is a source of error which is likely to

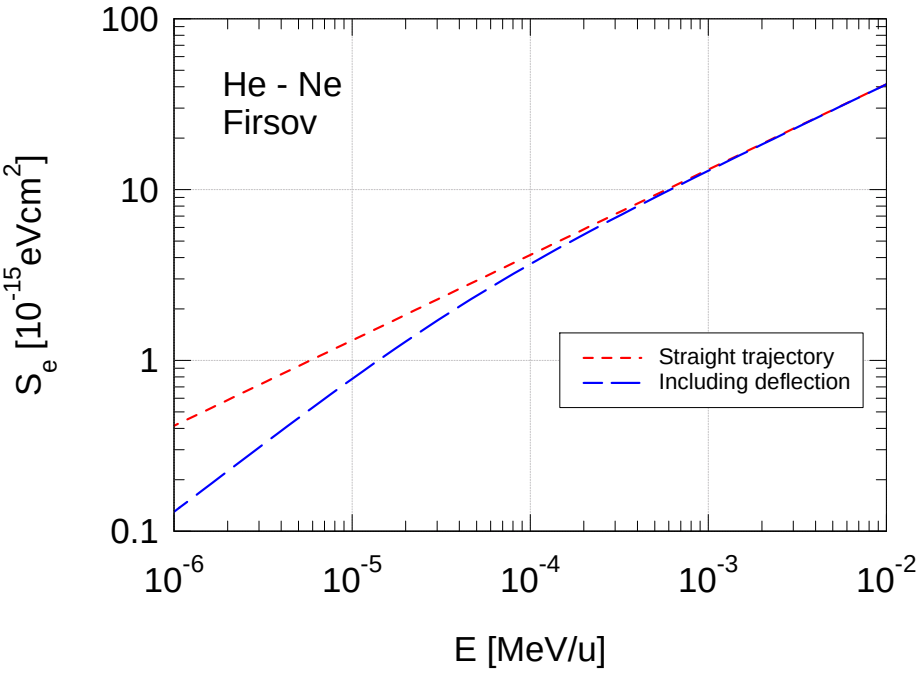

Figure 7: Comparison of calculated electronic stopping cross sections for straight and bent trajectory, He in Ne.

affect both our determination of I-values for heavy atoms and the comparison of calculated with measured stopping cross sections.

However, differences seen in Figure 1 between our I-values and those adopted in [7] are unrelated to relativity: Those I-values were determined by a procedure equivalent to ours but employing shell corrections based on hydrogenic, nonrelativistic wave functions and a Barkas-Andersen correction which is no longer up-to-date.

5.1.3. Threshold behavior, electron gas, Z_1 structure

The current version of PASS predicts velocity-proportional stopping from $v \lesssim v_0$ down to $v = 0$ for conductors, insulators and gas targets. While deviations from such behavior are evident in numerous experimental data, in particular from the groups in Linz and Bariloche discussed in refs. [54, 59], there are also theoretical reasons, depending on the electronic structure of the target. Here we mention an effect that causes deviations from velocity-proportional stopping for *all* materials.

Standard theory of electronic stopping assumes uniform projectile motion.

Exceptions are the low-velocity schemes by Firsov [62] and Kishinevskii [63] which, approximately, take into account that the projectile is deflected under a collision. This has the effect that there is a nonvanishing distance of closest approach, $R_{\min}(p, v)$, even at impact parameter $p = 0$. Figure 7 illustrates this effect on the example of He in Ne. It is seen that the Firsov formula predicts a significant correction from ~ 0.0001 MeV/u downward.

We are not yet able to produce a similar graph by PASS, but we have shown in ref. [54] that the effect of impact-parameter-dependent electronic energy loss is more pronounced when evaluated from PASS than from the Firsov formula. Therefore, as a matter of caution, the lower bound in the current DPASS compilation [15] has been set to 0.001 MeV/u.

Our stopping model for conduction electrons, which ignores the plasma mode, is clearly oversimplified. Standard theory [58] is readily applicable to H and perhaps He ions, but a nonlinear approach is needed for heavier ions. Relevant options have long been available in the literature [12]. Such an approach should account for Z_1 structure, 'Z_1 oscillations' in low-velocity stopping, first observed by Ormrod & Duckworth [64]. Several nonlinear theoretical schemes predict such oscillations [65, 66, 67], but all of them operate with an electron-gas target, yet equally pronounced Z_1 structure has been found in gas targets [68]. Here we still see an open end.

5.1.4. Screening, charge state, projectile excitation, electron capture and loss

PASS offers two options for projectile screening (exponential or Molière screening). Differences in the output have been found barely significant. We have kept exponential screening as the default.

PASS also offers two options for projectile excitation, bottom-up or distributed. There is a small but noticeable difference. Comparison with a few standard cases, especially O-Al, suggests a slight preference to the 'distributed' option which also appears more appropriate intuitively. This option, as well as exponential screening, also underlies the tabulations in ref. [13].

We have repeatedly explored various options for the mean equilibrium charge on PASS output [23, 69], and again in connection with the present study. Even though differences are significant, we still find that as long as all output is determined with a single jobfile, the simple Thomas-Fermi charge (10) is the best compromise.

PASS determines the energy loss at the mean charge instead of the mean value of the charge-dependent energy loss. This assumption is a significant source of error for light projectiles, mainly H, He and Li ions. A better solution, which also

affects projectile excitation and charge exchange, is on our road map.

5.2. Nuclear stopping, impact-parameter-dependent energy loss

On the experimental side we have paid attention to two significant sources of error, the necessary correction for nuclear stopping at low energies and the impact-parameter dependence of electronic energy loss.

In the literature we have identified papers that do not mention nuclear stopping at all [60]. More often, the description of the applied correction for nuclear stopping is incomplete [70], and cases have been identified, where the full nuclear stopping has been subtracted from the measured energy loss, neglecting the fact that when energy loss is measured in transmission, ions that experience large nuclear energy losses are deflected by large angles and do not enter the detector [54, 59]. In ref. [54] we discussed two ion-target combinations where we found that this action causes a rather sudden change of slope from a $\sqrt{E}$ to an approximately linear dependence on E of the deduced electronic stopping cross section.

A more general source of error is the neglect of the dependence of electronic energy loss on impact parameter in an individual ion-atom collision. We have studied this effect extensively for the most-frequently applied transmission technique for measuring electronic energy loss [54, 59, 60], but some influence is also expected on alternative techniques, including inversion of ion ranges.

In brief, the need to minimize nuclear stopping suggests to measure the energy loss of a narrow beam cone, so that the majority of elastically scattered ions are not recorded in the detector. However, ions scattered at a large angle experience relatively large electronic energy loss. Therefore, the recorded electronic energy loss will underestimate the actual electronic stopping cross section. This is the main reason why the vast majority of stopping data in the graphs shown above lie *below* the theoretical prediction.

We have shown in ref. [59] that this effect causes a change in slope of the stopping cross section versus energy, and that its magnitude depends on the opening angle ϕ of the detector and the target thickness x via $\xi = Nxa_0^2$, where N is the number of atoms per volume and a_0 the Bohr radius. Unfortunately, complete information on these two quantities is rarely found in the literature. The effect is most pronounced for thin targets. This means that its influence is greatest in measurements on gas targets, where thinner layers can be studied in practice. Numerous examples may be found in refs. [54, 59, 60].

We note that amongst numerous ion-target combinations considered in Figures 2-6, several have been analysed previously, such as H ions in N, Al, Si and Ag in [54], H-Au and Ni-Au in [59], as well as He-N, Ne-N and Si-Al in [60]. In

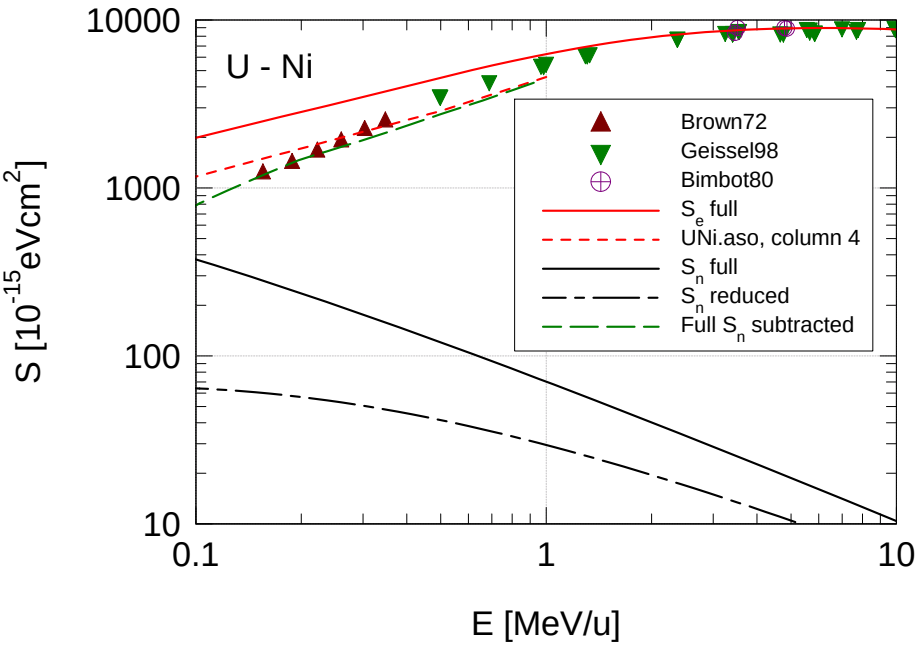

Figure 8: Electronic and reduced stopping for Au in Ni. $\phi = 0.02$, $\xi = 4$. See text.

Figure 8 we show that these effects also occur at relatively high energies for the heaviest projectiles. From 1 MeV/u down, the reduced stopping cross section (red dotted line) – which takes into account the p-dependence of electronic energy loss [54] – is seen to lie up to a factor of two below the unrestricted value (red solid line). The expected (restricted) nuclear energy loss (black dash-dotted line) is negligible, whereas the full nuclear energy loss (black solid line) is significant in the left half of the graph. The authors of ref. [71] have performed a correction for nuclear stopping on the basis of the unrestricted stopping cross section S_n full. It is seen that the dot-dashed green line, the difference between the reduced electronic stopping cross section – which we assert to be the quantity measured – and the full nuclear stopping cross section agrees well with the reported data.

6. Summary

- Output for almost 100 atom pairs (Z_1, Z_2), covering atomic numbers from 1 to 92 and an energy range from 100 eV/u to 1 GeV/u has been compared with experimental data extracted from the IAEA database [1].

- The main motivation for this study has been the wish to define a set of options to make PASS output freely available on the internet [15].

- For ions heavier than Li but lighter than Xe, agreement with experimental data is typically better than 5% above the Bragg peak and better than 20% around the Bragg peak. Major discrepancies at energies below the Bragg peak are ascribed primarily to the analysis of experimental data.

- For ions from Xe upward, in the energy range above the maximum, the agreement between PASS output and experimental stopping cross sections is typically within experimental scatter.

- Around the stopping maximum, PASS data tend to lie slightly below PASS predictions, although within (often quite large) experimental scatter in most cases.

- Good agreement is generally found below the stopping maximum down to the Bohr speed [69], with the exception of He and Li ions, where our description involving a mean charge state becomes questionable.

- Published data on stopping at velocities below the Bohr speed need special attention, since commonly applied procedures for data analysis treat

electronic energy loss as a friction force without attention to its impact-parameter dependence.

- In those cases that we have analyzed explicitly [54, 59, 60] and Figure 8, we argue that estimates from PASS come closer to the true electronic stopping cross section than do the reported values.

Cordial thanks are due to Valery Kuzmin for modifying his REST code to automatize the compilation of PASS stopping tables. This work has been supported by the Carlsberg Foundation.

References

[1] H. Paul, *Stopping power graphs*, URL `https://www-nds.iaea.org/stopping/`.

[2] L. C. Northcliffe and R. F. Schilling, Nucl. Data Tab. A 7 (1970) 233.

[3] F. Hubert, A. Fleury, R. Bimbot and D. Gardès, Ann. de Phys. 5 S (1980) 3.

[4] J. F. Janni, At. Data Nucl. Data Tab. 27 (1982) 147.

[5] J. F. Ziegler, *Particle interactions with matter* (2012), URL `www.srim.org`.

[6] F. Hubert, R. Bimbot and H. Gauvin, At. Data and Nucl. Data Tab. 46 (1990) 1.

[7] ICRU, *Stopping powers and ranges for protons and alpha particles*, vol. 49 of *ICRU Report* (International Commission of Radiation Units and Measurements, Bethesda, Maryland, 1993).

[8] H. Paul, *Program MSTAR* (2002), URL `https://www-nds.iaea.org/stopping/MstarWWW/MSTARInstr.html`.

[9] N. Bohr, Mat. Fys. Medd. Dan. Vid. Selsk. 18 no. 8 (1948) 1.

[10] U. Fano, Ann. Rev. Nucl. Sci. 13 (1963) 1.

[11] P. Sigmund, *Particle Penetration and Radiation Effects*, vol. 151 of *Springer Series in Solid-State Sciences* (Springer, Berlin, 2006).

[12] P. Sigmund, *Particle Penetration and Radiation Effects Volume 2*, vol. 179 of *Springer Series in Solid-State Sciences* (Springer, Heidelberg, 2014).

[13] ICRU, *Stopping of ions heavier than helium*, vol. 73 of *ICRU Report* (Oxford University Press, Oxford, 2005).

[14] P. L. Grande and G. Schiwietz, *CasP version 5.2* (2013), URL `http://www.helmholtz-berlin.de/people/gregor-schiwietz/casp_en.html`.

[15] A. Schinner and P. Sigmund, *DPASS*, URL `www.sdu.dk/DPASS`.

[16] P. Sigmund and A. Schinner, Europ. Phys. J. D 12 (2000) 425.

[17] N. Bohr, Philos. Mag. 25 (1913) 10.

[18] J. Lindhard, Nucl. Instrum. Methods 132 (1976) 1.

[19] F. M. Smith, W. Birnbaum and W. H. Barkas, Phys. Rev. 91 (1953) 765.

[20] H. H. Andersen, H. Simonsen and H. Sørensen, Nucl. Phys. A125 (1969) 171.

[21] H. Bethe, Ann. Physik 5 (1930) 324.

[22] F. Bloch, Ann. Physik 16 (1933) 285.

[23] P. Sigmund and A. Schinner, Nucl. Instrum. Methods B 195 (2002) 64.

[24] B. L. Henke, E. M. Gullikson and J. C. Davies, At. Data & Nucl. Data Tab. 54 (1993) 181.

[25] E. D. Palik, *Electronic handbook of optical constants of solids – version 1.0* (SciVision – Academic Press. San Diego, 2000).

[26] J. Berkowitz, *Photoabsorption, photoionization and photoelectron spectroscopy* (Academic Press, New York, 1979).

[27] J. Berkowitz, *Atomic and molecular photoabsorption. Absolute total cross sections* (Academic Press, San Diego, 2002).

[28] R. M. Sternheimer, M. J. Berger and S. M. Seltzer, Phys. Rev. B 26 (1982) 6067.

[29] R. M. Sternheimer, Phys. Rev. 88 (1952) 851.

[30] P. Sigmund, Phys. Rev. A 56 (1997) 3781.

[31] G. Molière, Z. Naturforsch. 2a (1947) 133.

[32] W. E. Lamb, Phys. Rev. 58 (1940) 696.

[33] D. Thomas (1997), URL `http://www.chembio.uoguelph.ca/educmat/atomdata/bindener/elecbind.htm`.

[34] K. Shima, T. Ishihara and T. Mikumo, Nucl. Instrum. Methods 200 (1982) 605.

[35] G. Schiwietz and P. L. Grande, Nucl. Instrum. Methods B 175-177 (2001) 125.

[36] A. Fettouhi, H. Geissel, A. Schinner and P. Sigmund, Nucl. Instrum. Methods B 245 (2006) 22.

[37] P. Sigmund and L. G. Glazov, Europ. Phys. J. D 23 (2003) 211.

[38] P. Sigmund, Europ. Phys. J. D 12 (2000) 111.

[39] M. C. Walske, Phys. Rev. 88 (1952) 1283.

[40] P. Sigmund, Phys. Rev. A 26 (1982) 2497.

[41] E. Clementi and C. Roetti, Atomic Data & Nucl. Data Tables 14 (1974) 177.

[42] F. Herman and S. Skillman, *Atomic structure calculations* (Prentice Hall, New Jersey, 1963).

[43] N. Bohr, Philos. Mag. 30 (1915) 581.

[44] H. Bethe, Z. Physik 76 (1932) 293.

[45] J. Lindhard and A. H. Sørensen, Phys. Rev. A 53 (1996) 2443.

[46] W. H. Bragg and R. Kleeman, Philos. Mag. 10 (1905) 318.

[47] P. Sigmund and A. Schinner, Nucl. Instrum. Methods B 415 (2018) 110.

[48] M. S. Weng, A. Schinner, A. Sharma and P. Sigmund, Europ. Phys. J. D 39 (2006) 209.

[49] P. Sigmund and A. Schinner, Nucl. Instrum. Methods B 258 (2007) 116.

[50] P. Sigmund and A. Schinner, Europ. Phys. J. D 23 (2003) 201.

[51] A. Schinner and P. Sigmund, Europ. Phys. J. D 56 (2010) 41.

[52] P. Sigmund and A. Schinner, Europ. Phys. J. D 56 (2010) 51.

[53] P. Sigmund and A. Schinner, Europ. Phys. J. D 58 (2010) 105.

[54] P. Sigmund and A. Schinner, Nucl. Instrum. Methods B 410 (2017) 78.

[55] ICRU, *Stopping powers for electrons and positrons*, vol. 37 of *ICRU Report* (International Commission of Radiation Units and Measurements, Bethesda, Maryland, 1984).

[56] H. H. Andersen, H. Sørensen and P. Vajda, Phys. Rev. 180 (1969) 373.

[57] R. Ishiwari, N. Shiomi, S. Shirai and U. Uemura, Phys. Lett. A 48 (1974) 96.

[58] J. Lindhard, Mat. Fys. Medd. Dan. Vid. Selsk. 28 no. 8 (1954) 1.

[59] A. Schinner and P. Sigmund, Nucl. Instrum. Methods B in press (2018).

[60] P. Sigmund, V. Kuzmin and A. Schinner, Nucl. Instrum. Methods B ICACS volume (2018) submitted.

[61] P. Børgesen, H. M. Chen and H. Sørensen, Nucl. Instrum. Methods 194 (1982) 71.

[62] O. B. Firsov, Zh. Eksp. Teor. Fiz. 36 (1959) 1517, [Engl. transl. Sov. Phys. JETP **9**, 1076-1080 (1959)].

[63] L. M. Kishinevskii, Izv. Akad. NAUK SSSR 26 (1962) 1410, [Engl. transl. Bull. Acad. Sci. USSR Phys. Ser. **20**,1433-1438 (1963)].

[64] J. H. Ormrod and H. E. Duckworth, Can. J. Phys. 41 (1963) 1424.

[65] J. S. Briggs and A. P. Pathak, J. Phys. C 7 (1974) 1929.

[66] P. M. Echenique, R. M. Nieminen and R. H. Ritchie, Sol. St. Comm. 37 (1981) 779.

[67] N. R. Arista, Nucl. Instrum. Methods B 195 (2002) 91.

[68] P. Hvelplund, Mat. Fys. Medd. Dan. Vid. Selsk. 38 no. 4 (1971) 1.

[69] P. Sigmund and A. Schinner, Nucl. Instrum. Methods B 342 (2015) 292.

[70] L. G. Glazov and P. Sigmund, Nucl. Instrum. Methods B 207 (2003) 240.

[71] M. D. Brown and C. D. Moak, Phys. Rev. B 6 (1972) 90.